Check for updates

Microstructure-dependent particulate filtration using multifunctional metallic nanowire foams†

James Malloy, [a] Erin Marlowe, [a] Christopher J. Jensen, [a] Isaac S. Liu, [a,b] Thomas Hulse, [a,c] Anne F. Murray, [d] Daniel Bryan, [d] Thomas G. Denes, [d] Dustin A. Gilbert, [e] Gen Yin [a] and Kai Liu *[a]

The COVID-19 pandemic has shown the urgent need for the development of efficient, durable, reusable and recyclable filtration media for the deep-submicron size range. Here we demonstrate a multifunctional filtration platform using porous metallic nanowire foams that are efficient, robust, antimicrobial, and reusable, with the potential to further guard against multiple hazards. We have investigated the foam microstructures, detailing how the growth parameters influence the overall surface area and characteristic feature size, as well as the effects of the microstructures on the filtration performance. Nanogranules deposited on the nanowires during electrodeposition are found to greatly increase the surface area, up to 20 m^2 g^{-1}. Surprisingly, in the high surface area regime, the overall surface area gained from the nanogranules has little correlation with the improvement in capture efficiency. However, nanowire density and diameter play a significant role in the capture efficiency of $PM_{0.3}$ particles, as do the surface roughness of the nanowire fibers and their characteristic feature sizes. Antimicrobial tests on the Cu foams show a >99.9995% inactivation efficiency after contacting the foams for 30 seconds. These results demonstrate promising directions to achieve a highly efficient multifunctional filtration platform with optimized microstructures.

Introduction

Ultrasmall airborne particulates pose potentially severe health risks due to their ability to penetrate deep into the respiratory system, from the transmission of infections such as COVID-19 to air pollution.[1–4] One of the most effective methods of combating the spread of COVID-19 has been the use of high efficacy face masks to prevent the inhalation of viral particles attached to ultrasmall aerosols and droplets.[5–7] A variety of materials have been used for particulate filtration, such as cotton, fiberglass, and polypropylene. Cotton is inexpensive but has a low filtration efficiency;[2] fiberglass has a high filtration efficiency but is not structurally stable enough to be used as a face respirator;[8] and polypropylene (used in N-95 respirators) has a high filtration efficiency but cannot be easily cleaned, reused or recycled, due to the reliance on electrostatics. One of the major drawbacks of using disposable face masks has been the environmental toll,[9–11] with an estimated average 1.6 million metric tons of plastic being discarded every day during the pandemic.[12] It is critically important to develop reusable, efficient and robust filters for submicron airborne particulates, especially for protection against COVID-19 and other infectious diseases.

Many novel filter materials have been studied in light of the COVID-19 pandemic, including electrostatically charged Polyvinylidene fluoride (PVDF) nanofibers,[13] nanoparticle imbedded protein nanofibrils,[14] Ag-imbedded polymers,[15–17] porous metal–organic frameworks (MOFs),[18–21] and carbon nanotubes.[22–24] Metallic filtraton media with no polymer components are particularly promising, as they can withstand high temperatures, ionizing radiation, and exposure to oils, all of which cause polymers to rapidly degrade.[25–27] Conventional porous metal foams often utilize sizable building blocks, with micron-scale dimensions and larger, which are inefficient against deep-submicron particulates that are the hardest to capture.[28,29] Recently advances in metallic nanowire networks and foams offer a promising new platform for explorations in catalysis, gas storage, nanomagnetics and neuromorphic computing.[30–35] However, most such metallic monoliths are not mechanically robust enough to be useful as practical filters. It is challenging to realize nanoporous metallic foams that maintain nanoscale dimensions, which are essential for deep micron particulate filtration, and are also mechanically robust.

Previously, we have demonstrated that nanowire-based low-density metal foams, synthesized by electrodeposition and sin-

*a*Department of Physics, Georgetown University, Washington, DC 20057, USA. E-mail: kai.liu@georgetown.edu

*b*Department of Computer Science, Vanderbilt University, Nashville, TN 37235, USA

*c*Department of Physics, University of Louisville, Louisville, KY 40292, USA

*d*Department of Food Science, University of Tennessee, Knoxville, TN, 37996, USA

*e*Department of Materials Science and Engineering, University of Tennessee, Knoxville, TN 37996, USA

tering, are robust enough to withstand air speeds of over 20 m s^{-1} and pressure differentials of over several atmospheres without showing any sign of deformation or degradation.[36] Further, they also exhibit extremely large surface areas as well as outstanding filtration efficiencies (>96.6%) in the $PM_{0.3}$ regime with breathability comparable to N-95 respirators.[36] They can also be easily cleaned[36] and decontaminated[37] to allow sustained use, and eventually recycled at the end of their useful lifetime.[38]

Despite the promising initial results on such nanoporous metallic foams, a quantitative understanding of how the synthesis conditions and foam microstructures affect the filtration performance is still lacking. To enhance the foam mechanical stability, a second electrodeposition process was used to reinforce the intersections of the Cu foams.[36] An accompanying effect is a significant change in the foam surface areas and morphology due to nanogranule growths along the nanowires. In such 3D interconnected foams, it is critical to understand the correlation between the foam microstructures and the filtration performance.

In this study we have quantitatively investigated how the nanoporous foam microstructures impact the filtration performance, particularly against particulates that are around 0.3 μm in size used in standardized filtration efficiency tests.[28,29] We distinguish the effects of surface area enhancement vs. the density of nanoscale feature sizes comparable to the particulates being filtered. Interestingly, while foam surface areas are generally important for filtration efficiency, for high surface areas in the range of 1 m^2 g^{-1} and beyond, the sizes of the foam surface features play a more prominent role. These results demonstrate nanoporous metallic nanowire foams as a multi-functional platform for deep submicron particulate filtration that is efficient, robust, antimicrobial, and reusable, with the potential to further guard against multiple hazards.

Results and discussion

Synthesis and foam morphology

Nanoporous copper foams were fabricated using electrodeposited nanowires (NWs) following a cross-linking and freeze-drying technique, as described previously.[31,36] Anodized aluminum oxide (AAO) templates with 200 nm pore size and 60 μm thickness were used for the electrochemical deposition (ED) of Cu NWs.[34,39,40] Subsequently, NWs were liberated from the AAO membrane into deionized water. The NW–water suspension was freeze-cast by liquid nitrogen into the desired shape and then pumped in vacuum to sublimate the ice. The resultant free-standing foam was strengthened by sintering at 300 °C, while simultaneously undergoing multiple oxidation/reduction cycles.[36,41] Here, foams with an initial density $\rho_i \sim$ 2–3% of the Cu bulk density were achieved after this first synthesis step of ED and sintering. Such foams have extremely large surface area-to-volume ratios, up to $10^6 : 1$ m^{-1}.[31]

Subsequently, the foams were strengthened further using a secondary electrodeposition (2ED) step to achieve a final density ρ_f, in a bath of copper sulfate along with a mixture of leveler, accelerator, and suppressor compounds to ensure even and homogeneous plating.[36] The resulting foams were significantly stronger and more durable due to increased bonding areas at intersections of nanowires, while still retaining a high surface area and an excellent filtration efficiency.[36]

The morphology of the foams varied widely depending on the amount of secondary electroplating as well as other factors (Fig. 1). As the 2ED process began, small nanogranules started to deposit along the surface of the NWs (Fig. 1a, for a ρ_f = 2.2% density foam). As the amount of copper plated increased, these nanogranules began to increase in size (Fig. 1b, for a ρ_f = 5% density foam). With enough plating, e.g., for a foam with a ρ_f = 30% density, the nanogranules eventually coalesced together, enclosing multiple nanowires into larger filaments with smoother surfaces (Fig. 1c). The foam microstructures could be further tuned by the electrolyte conditions, e.g., lowering the pH value of the solution reduced the nanograin feature size deposited on the nanowire surface and increased the overall surface smoothness (see ESI†). Final optimized foams exhibit both low density and strong mechanical strength that are essential for filtration media applications (Fig. 2a and b).

Pressure differential and breathability

One of the most important characteristics of a filter is its breathability, which is inversely proportional to the pressure drop across the foam (ΔP). The ΔP quantity is measured experimentally by flowing air through the foam as a function of air velocity and measuring the difference between the pressure upstream and downstream of the foam (ESI†). It was shown previously[36] that $\Delta P = Av + Bv^2$, where v is the velocity of the airflow, and A and B are constants determined by the properties and geometry of the foam.[42] As most filters operate in the low velocity regime where $v \approx 0.05$ m s^{-1}, the linear term is the dominant one,[43] or $\Delta P \approx Av$. Thus, it is more useful to evaluate the pressure drop coefficient $\Delta P/v$ for our foam samples with various ρ_i, ρ_f and thickness (t), as shown in Table 1 and Fig. 2c.

For comparison, an N-95 respirator has a pressure drop coefficient of around 1.0 kPa m^{-1} s.[36] Our ρ_f = 15% foams (sample 7, $\Delta P/v$ = 0.97 ± 0.11 kPa m^{-1} s) were found to have breathability comparable to an N-95, while also being lightweight enough to rest comfortably on the tip of a feather (Fig. 2a) and structurally robust enough to support a 1.8 kg weight without collapse or deformation (Fig. 2b). Most of our 1 mm thick foams with $\rho_f \leq 15\%$ (samples 1–7) exhibit excellent breathability, which improves as foam thickness and packing density decrease, with the ultra-low density ρ_f = 3.5% foam (Table 1, sample 1, $\Delta P/v$ = 0.48 ± 0.04 kPa m^{-1} s) being over twice as breathable as an N-95 ($\Delta P/v$ = 1.02 ± 0.02 kPa m^{-1} s). This overall trend is also illustrated in Fig. 2 (blue bins), which reveal a few trends: (1) an inverse proportionality between breathability and filter thickness is clearly seen for foams with the same initial and final densities (sample 7 vs. 8). (2) For foams with the same initial density ρ_i and thickness (sample #1 vs. 2, #6 vs. 7 and 9), the higher the final density ρ_f,
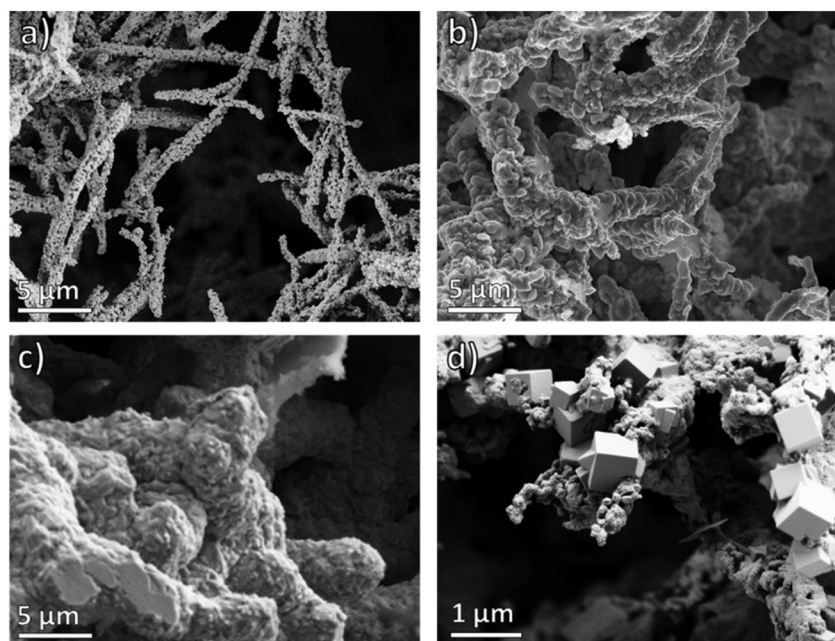
Fig. 1 Foam microstructure evolution with synthesis conditions. SEM Images of 2ED (a) 2.2%, (b) 5.0%, and (c) 30% density foams, illustrating the evolution of foam morphology. With continued electrodeposition, the nanogranules along the nanowires grow larger, eventually coalesce into a thicker coating along the nanowires, even forming large filaments as shown in panel (c). (d) Cubical NaCl crystals captured in a 5.0% density foam.
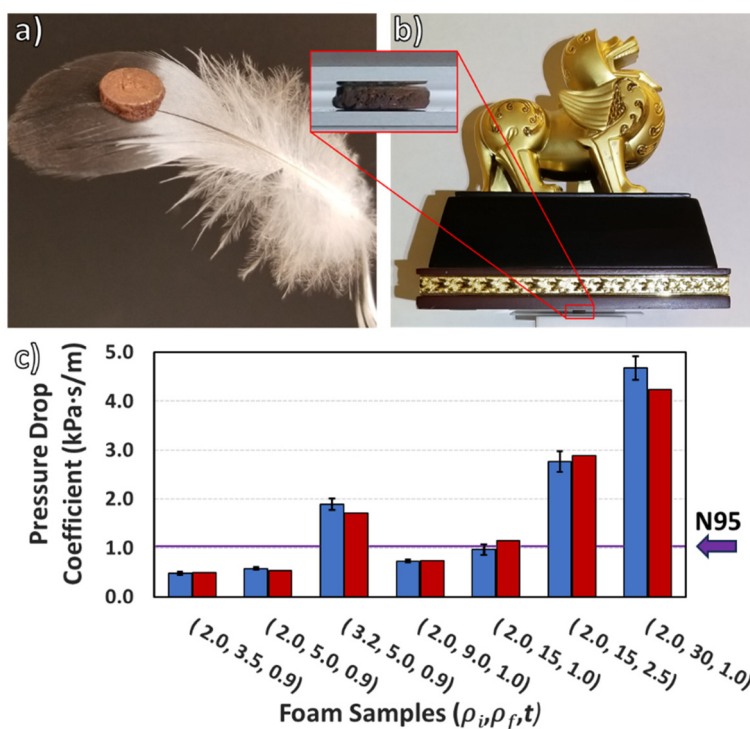

Fig. 2 Robust and breathable light-weight foam. (a) A 120 mg 15% bulk density foam 9 mm in diameter resting on the tip of a feather. (b) The same foam supporting a 1.8 kg weight. (c) Comparison of measured (blue) vs. calculated (red) breathability for foam samples with various initial density ρ_i (%), final density ρ_f (%), and thickness t (mm). A 15% bulk density foam (sample 7) similar to the one pictured in panels (a) and (b) has a comparable breathability to an N-95 respirator (purple line). Panels (a) and (b) adapted with permission of ASM International, from Ref. 41.

the larger the $\Delta P/v$, indicating that the additional Cu deposited during the 2ED process is generally impeding the air flow. (3) Interestingly, for foams with the same final density ρ_f

and thickness, sample 4 with ρ_i of 3.2% has a $\Delta P/v$ that is more than 3 times that of sample 2 with ρ_i of 2.0%. Both samples were made with the same starting 200 nm diameter

Table 1 Foam filtration characteristics[a]

Sample ID	ρ_i (%)	ρ_f (%)	t (mm)	$\Delta P/v$ (kPa m^{-1} s)	Efficiency (%) (measured)	F_{QE}	F_{QC}	F_{QC} error (%)	F_{QSF}	$Q_{Measured}$	$Q_{Calcu.}$
1	2.0	3.5	0.9	0.48 ± 0.04	91.0 ± 0.1	2.41 ± 0.01	2.59	7.5	2.43	5.02 ± 0.41	4.87
2	2.0	5.0	0.9	0.58 ± 0.03	84.2 ± 3.0	1.85 ± 0.19	1.98	7.0	1.87	3.19 ± 0.36	3.47
3	2.5	5.4	1.0	—	92.5 ± 0.1	2.59 ± 0.01	2.92	13	—	—	—
4	3.2	5.0	0.9	1.88 ± 0.12	99.0 ± 0.1	4.61 ± 0.10	3.95	−14	4.56	2.45 ± 0.15	2.68
5	2.5	6.8	1.0	—	89.1 ± 0.1	2.22 ± 0.09	2.60	17	—	—	—
6	2.0	9.0	1.0	0.73 ± 0.03	81.1 ± 0.5	1.67 ± 0.02	1.62	−3.0	1.71	2.29 ± 0.10	2.31
7	2.0	15	1.0	0.97 ± 0.11	76.8 ± 1.3	1.46 ± 0.05	1.25	−14	1.41	1.51 ± 0.18	1.22
8	2.0	15	2.5	2.76 ± 0.21	96.6 ± 2.0	3.38 ± 0.67	3.13	−7.4	—	—	—
9	2.0	30	1.0	4.67 ± 0.24	54.2 ± 0.5	0.78 ± 0.01	0.88	13	0.77	0.17 ± 0.01	0.18

[a] Including $\frac{\Delta P}{v}$; measured $PM_{0.3}$ filtration efficiency; measured, calculated and surface-feature corrected filtration qualities (F_{QE}, F_{QC} and F_{QSF} respectively); and the measured and calculated quality factors Q.

Cu nanowires, however sample 4 was fabricated with a greater number density of nanowires which results in a significantly increased nanowire length density compared to sample 2. Further, the amount of Cu plated onto sample 4 per nanowire during the 2ED stage is significantly less than in sample 2, which results in smaller final diameter nanowires. Both the increased nanowire length density and the decreased nanowire diameter in sample 4 contribute to a higher pressure drop due to the increased surface area per filter volume which induces more drag.[44]

To gain a quantitative understanding of the exact relationship between breathability and nanowire diameter and foam initial/final densities, as a crude first approximation, we may consider the foams as a simple compilation of isolated cylindrical fibers with smooth surfaces, even though the actual foams are more complex interconnected 3D nanowire networks with various surface details. Single fiber theory for the pressure drop,[44] combined with the Miyagi model[45] for the pressure drop across an array of fibers allows us to express the linear pressure drop coefficient as (derivation in ESI†):

$$\frac{\Delta P}{v} = -C \frac{\rho_i^{\frac{5}{2}} \cdot e^{4.75\rho_f} \cdot t}{\rho_f^{\frac{1}{2}} \cdot \left[\ln(\rho_f) + \frac{1 - \rho_f^2}{1 + \rho_f^2}\right]} \qquad (1)$$

Remarkably, with this substantial simplification, the calculated pressure drop is quite comparable to the measured results (Fig. 2c). This agreement suggests that pressure drop scales linearly with filter thickness (t) and increases substantially as the initial nanowire number density ($\propto \rho_i$) and final density (ρ_f) go up. By fitting eqn (1) across a range of foam samples, the scaling factor C is determined to be 3.64×10^6 kPa m^{-2} s.

Filtration efficiency

Foam samples of varying thicknesses, ρ_i and ρ_f are used to filter aerosolized 0.3 μm NaCl particles, and the overall filtration efficiency is measured using a TSI AeroTrak® Portable Particle Counter Model 9110 (ESI†). A few clear trends can be seen between samples that only differ by one parameter (Table 1). For instance, for foams with the same microstruc-

tures (e.g., samples 7 and 8), a thicker filter is indeed more efficient; for foams with the same ρ_i and t, smaller ρ_f leads to a higher filtration efficiency (samples 6, 7, and 9). Interestingly, for foams with the same ρ_f and t, sample 4 with a higher ρ_i of 3.2% exhibits a higher filtration efficiency of 99.0%, as compared to sample 2 (ρ_i = 2.0%, with an 84.2% efficiency). While the correlation between filter thickness with filtration efficiency is well understood, the relationship between the foam density and other key microstructure characteristics with filtration efficiency is less clear.

To evaluate the correlation between the foam microstructure and filtration efficiency, we will first model the capture efficiency using basic air filtration theory for a perfectly smooth fiber. The filtration quality of a material is defined as a dimensionless quantity $F_Q \equiv -\log(1 - E)$, where E is the filtration efficiency.[2,44] An N-95 respirator is certified to have a F_Q of at least 3.0 for particles in every size range, while an N-99 respirator has a F_Q of at least 4.6.[46] Using the smooth fiber model,[3,44] the filtration quality can be written as (see ESI†):

$$F_Q \sim \frac{n \times t}{d_f} = k_E \frac{\rho_i^{\frac{3}{2}} \cdot t}{\rho_f^{\frac{1}{2}}} \qquad (2)$$

where n is the length density of the nanowires in the foam, or the sum of the lengths of all the nanowires per given volume, and it scales with ρ_i; d_f is the final average nanowire diameter after electrodeposition and scales as $d_f \propto \sqrt{\frac{\rho_f}{\rho_i}}$, and finally k_E is a constant dependent on a multitude of factors such as filtration material, fiber geometry, and other testing conditions that affect filtration efficiency. As it is more useful to evaluate how far off proportionally the calculated filtration quality (F_{QC}) is from experimentally measured filtration quality (F_{QE}), rather than the difference between the two values, we fit k_E to minimize $\sum \left(\frac{F_{QC}}{F_{QE}} - \frac{F_{QE}}{F_{QC}}\right)^2$. This ensures that foams with larger thicknesses or otherwise have higher filtration qualities are not weighted disproportionately, and that the percentage error between F_{QE} and F_{QC} are minimized with equal weight across all ranges of foam samples with varying filtration qualities.

The best fit for the smooth fiber model described in eqn (2) was determined to be k_E = 171.5 mm^{-1}.

As shown in Table 1, the smooth fiber model alone can be used to describe the filtration quality of the foam filters to within an error of ±17%. With a theoretical baseline for how well perfectly smooth fibers capture particles, we can now determine *to what extent surface features contribute towards particulate filtration*. It is well established that a rougher fiber surface improves filtration capture efficiency,[47–49] which is intimately coupled with an increase in surface area and the foam microstructure. Initially the nanowires which comprise the foam have a relatively smooth surface structure as they were grown in an anodized aluminum oxide mold. However, during the 2ED process the deposition of Cu nanogranules on the surface of the nanowires begin to dramatically increase the surface area. Surface area was measured to high accuracy (<0.5% error) with a BET krypton adsorption isotherm. It was found that foams that were initially ~3% bulk density pre-2ED exhibit a maximal surface area of 20 m^2 g^{-1} for a 13% bulk density after 2ED. The surface area was found to initially increase as the relative density increases, with the percentage density increase being measured in coulombs of copper deposited during the 2ED process per mg of 1ED foam (Fig. 3a). In foams with an even higher density, the deposited nanogranules begin to coalesce into a smoother surface structure and the surface area decreases.

Previously we have observed a substantial drop in filtration efficiency in the ρ_f = 30% foam, whose surface area is more than an order of magnitude smaller than other foams with a lower ρ_f. It is interesting to examine any direct correlation between surface area and filtration efficiency. With the 2ED process, it was found that the deposited surface features increase the internal surface area of the foam substantially, some by over a factor of 10 higher than what is predicted by the smooth fiber model, *e.g.*, the aforementioned sample with a 20 m^2 g^{-1} surface area. To determine how much the increased surface area from the foam's surface features might influence capture efficiency, additional surface area from 2ED is compared with the smooth fiber filtration quality model, as illustrated in Fig. 3b.

Correlation with foam surface area and microstructure

Interestingly, for foams with surface area in the >1 m^2 g^{-1} range, the additional surface area contribution from 2ED has no appreciable correlation with the capture efficiency of 300 nm sized particles, as a linear regression model yields a r^2 value of 2×10^{-5}. This suggests that surface roughness and the surface area it adds as a stand-alone metric does not inherently aid in particle capture efficiency. But rather, there must be an additional characteristic of surface roughness that is required for filtration efficiency improvement. It has been shown on flat 2D surfaces that particles are captured more easily when they can nest into similarly sized crevices which increase the area of contact between the particle and substrate, leading to a higher sticking coefficient.[50] This can be seen in Fig. 1d, where the NaCl crystals tend to be wedged into comparably sized crevices which gives a higher area of contact. Therefore, we want to test how crucial of a role the *size* of the features deposited onto the fiber surface plays in influencing filtration efficiency.

Image analysis on SEM micrographs was performed on foam samples of various densities to determine the feature size distribution across samples. After preprocessing to remove the blurry background, an auto-local-threshold filter is applied to extract and measure the size and frequency of the nanogranule deposits along the nanowire surface (more details in ESI†). From this we can determine the feature size distribution across various samples, as illustrated in Fig. 4.

The increased particle capture due to nesting is maximized when surface features along the nanowires are similar in size to the particles being captured, and becomes diminished as the surface features become too large or too small relative to the particles. While the theoretical smooth fiber model pro-
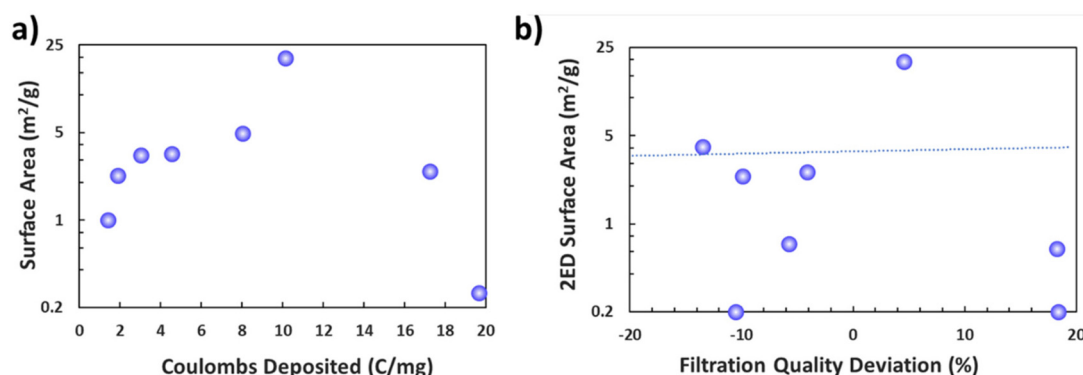

Fig. 3 Surface area correlation with filtration performance. (a) Surface area of the foams *versus* the relative amount of copper deposited during the 2ED step (coulombs deposited per mg of 1ED foam). Surface area begins to increase as deposited nanogranules along the nanowire surface increase overall surface roughness, up to around 20 m^2 g^{-1}. Somewhere after this point, nanogranules begin to coalesce into a smoother surface structure with reduced surface area. (b) Filtration quality deviation showing no obvious correlation ($r^2 = 2 \times 10^{-5}$) with the increased surface area contributed from deposited surface features.
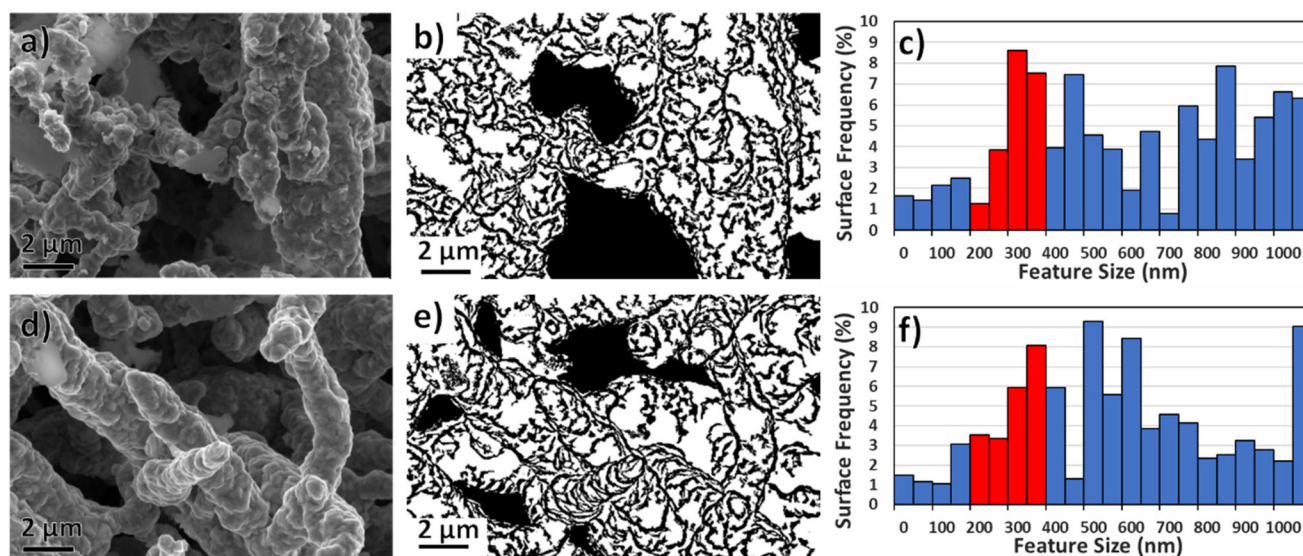
Fig. 4 Foam nanogranule size analysis. Image analysis performed on interiors of (a–c) ρ_f = 9% and (d–f) 17% foams, showing (a and d) SEM images, (b and e) images with thresholding, and (c and f) feature size distribution histograms with features between 200–400 nm highlighted in red.
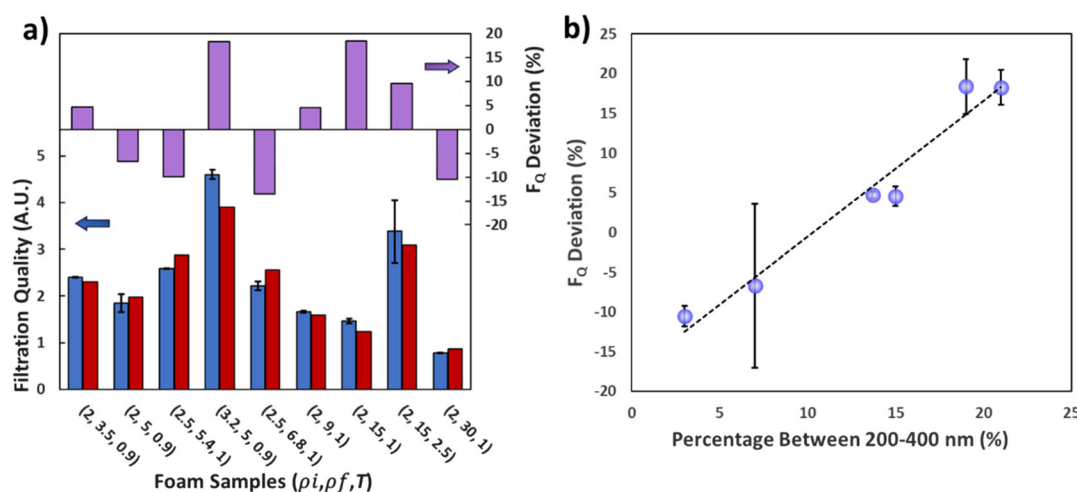

Fig. 5 Filtration quality dependence on foam microstructures. (a) Measured (blue) *versus* calculated (red) filtration quality histogram and filtration quality deviation (purple) between measured and calculated values. (b) High correlation (r^2 = 0.96) between filtration quality deviation and percentage of surface features between 200–400 nm.

vides a good fit to the experimental results (Fig. 5a), there are still appreciable differences due to surface features. To determine what the capture efficiency contribution is from the surface features, we can cross-reference the percentage of surface features in the 200–400 nm size range (Fig. 5b) with the filtration quality deviation between our measured results and the smooth fiber model (Fig. 5a).

By directly comparing the deviation in filtration quality for 300 nm sized particles between our measured results and the calculated smooth fiber model to the percentage of surface area that has surface features between 200–400 nm in size, we find that there is a very high correlation with the r^2 value of 0.96 in a simple linear regression model, as shown in Fig. 5b.

This suggests that the size of the surface structure plays a prominent role in increasing filtration efficiency, with some samples showing over a 30% increase in filtration quality compared to smooth fibers. Furthermore, the filtration efficiency dependence on feature size provides an explanation for why rough surfaces and high surface area do not necessarily result in an increase to capture efficiency. This can be understood as much of the added surface area from the 2ED process is primarily from ultrasmall surface features that are simply too small relative to the 300 nm sized particles to enhance particle capture efficiency *via* nesting, and also too small to change the geometry of the fiber to increase capture through diffusion or interception.

By approximating a linear relationship with the percentage increase in filtration quality and percentage of surface structures in the 200–400 nm range, a surface feature adjusted filtration quality can be derived as

$$F_{QSF} = 142 \cdot \frac{\rho_i^{\frac{3}{2}} \cdot t}{\rho_f^{\frac{1}{2}}}(1 + 0.019P) \quad (3)$$

where P is the percentage of surface area that has 200–400 nm sized surface features, and t in mm. This equation yields an excellent fit with our measured results, with a linear regression model r^2 value of 0.999. Using both eqn (3) and (1), we may now calculate the quality factor (Q) of the foams as

$$Q \equiv \frac{v \cdot F_{QSF}}{\Delta P} = -0.039 \frac{\left[\ln(\rho_f) + \frac{1 - \rho_f^2}{1 + \rho_f^2}\right] \cdot (1 + 0.019P)}{\rho_i \cdot e^{4.75\rho_f}} \quad (4)$$

This allows us to optimize the quality factor of the foam by tuning the initial and final densities of the foam. This can be seen in Table 1 where an ultra-low density 3.5% density foam (sample 1) was able to achieve a quality factor of 5.02, over 50% better than a standard N-95 respirator which has a quality factor of around 3.20.[36]

Note that our study has mostly focused on studying the effects of the nanowire length density, plating ratio during the 2ED stage, and surface features. There are a number of other parameters that can also influence both breathability as well as filtration efficiency that remained constant throughout the range of samples measured. As such, their contributions to filtration efficiency and breathability could be absorbed into the fitted proportionality constant. For instance, the spacing geometry of the NWs is important. When the NWs bundle together such that they create large pockets absent of NWs, the breathability increases dramatically. However, this benefit is offset by the significant drop in filtration efficiency. Similarly, the studies were carried out on samples that were in the density range of being structurally stable and NWs being relatively inflexible. While the derived equations would suggest that ultra-low-density foams would have an extremely high breathability and quality factor, it was found experimentally that at densities below 3% the NWs begin to collapse, limiting both breathability and filtration efficiency. Additionally, while the derived quality factor equation suggests that extremely high-quality factors can be achieved by reducing the NW density, realistically at these limits, the heavily diminished structural integrity and changes to NW spacing begins to play a non-negligible role which causes the quality factor to decrease. Additionally, the choice of NW materials may affect both the sticking coefficient of airborne particles and the rigidity of the foams, which are relevant to the pressure drop as well as filtration quality, which is of interest for future studies.

Another important functionality of the foams is its antimicrobial characteristics. Once captured, conventional filter materials sequester the live pathogens, which can survive in the respirator. This makes the used filter material a potential hazard as the pathogens can be released from the filter through rough handling.[51] Copper, being a bioactive metal with antimicrobial properties achieved through surface contact,[52] is expected to be self-sterilizing, killing captured bacteria and inactivating captured viruses.[15,53] Antimicrobial testing was performed on our Cu foams using a contact assay described previously.[52] In these tests, 10 µL of a concentrated solution containing the bacteriophage Phi6 was deposited on the surface of the foam, then a glass slide was set on top of the droplet to disperse the solution across a 6.4 cm^2 area. After 30 seconds, the slide was removed and the solution was washed from the foam using 990 µL of phosphate buffer solution, which was collected in a Petri dish. The solution was then enumerated by double-layer agar plating using its host bacteria *Pseudomonas syringae*. The bacteriophage Phi6 has a similar structure to SARS-CoV 2, including a double capsid lipid–protein envelope and protruding spike proteins. Bioactivity from a stainless steel coupon was also measured as a negative control. Each test was performed in triplicate.

The copper foam resulted in a 6.7 ± 1.3 log-reduction of the active bacteriophage, corresponding to a >99.9995% inactivation efficiency in the 30 seconds test. These results are consistent with the strong bioactivity of copper and demonstrate that this bioactivity extends to the nanostructured material. Functionally, these results confirm that captured pathogens will become inactivated soon after contacting the Cu superstructure.

Conclusion

We have demonstrated nanoporous metallic nanowire foams as a smart, multifunctional platform for deep submicron particulate filtration that is efficient, robust, antimicrobial, and reusable, with the potential to further guard against multiple hazards. By tuning the 2ED process to maximize the amount of deposited nanogranules and surface area, foams with surface areas of 20 m^2 g^{-1} have been achieved, with breathability comparable to an N-95 respirator. Furthermore, we have shown how foam microstructures, including NW length density and the 2ED surface feature distribution, influence the capture efficiency. We have shown that overall surface roughness and its contribution to surface area is only a partial requirement for increasing filtration efficiency, and that the size of the surface features plays a pivitol role as well. This suggests that our foams, as well as other conventional filters, can be further improved by optimizing the size scale of the surface roughness of the fibers to capture 0.3 µm sized particles. By adjusting growth parameters and increasing the amount of ~0.3 µm sized surface features, the capture efficiency of a 0.9 mm thick 5% density foam is increased from 84% to over 99% for the PM$_{0.3}$ regime, and the filtration quality factor can be enhanced by over 30%, with room for further increase. Antimicrobial tests on the Cu foams demonstrate a >99.9995% inactivation efficiency after contacting the foams for 30 seconds. These results demonstrate promising

directions to achieve a highly efficient multifunctional filtration platform with optimized microstructures.

Author contributions

J. M. and K. L. conceived the concept and K. L. coordinated the project. J. M. led the sample synthesis, microstructure characterizations, filtration measurements and data analysis, together with E. M., C. J. J., I. S. L., T. H., G. Y. and K. L., I. S. L. and G. Y. performed imaging analysis. A. F. M., D. B., T. G. D. and D. A. G. performed antimicrobial tests. J. M. and K. L. wrote the first draft of the manuscript. All authors contributed to the revision.

Data availability

The data supporting this article have been included as part of the ESI.†

Conflicts of interest

J. M. and K. L. are coinventors on a filed patent application by Georgetown University on *Nanoporous metal foam gas and fluid filters*.

Acknowledgements

References

1 L. Liao, W. Xiao, M. Zhao, X. Yu, H. Wang, Q. Wang, S. Chu and Y. Cui, Can N95 Respirators Be Reused after Disinfection? How Many Times?, *ACS Nano*, 2020, **14**(5), 6348–6356.

2 A. Konda, A. Prakash, G. A. Moss, M. Schmoldt, G. D. Grant and S. Guha, Aerosol Filtration Efficiency of Common Fabrics Used in Respiratory Cloth Masks, *ACS Nano*, 2020, **14**(5), 6339–6347.

3 C. D. Zangmeister, J. G. Radney, E. P. Vicenzi and J. L. Weaver, Filtration Efficiencies of Nanoscale Aerosol by Cloth Mask Materials Used to Slow the Spread of SARS-CoV-2, *ACS Nano*, 2020, **14**(7), 9188–9200.

4 H. R. Lee, L. Liao, W. Xiao, A. Vailionis, A. J. Ricco, R. White, Y. Nishi, W. Chiu, S. Chu and Y. Cui, Three-Dimensional Analysis of Particle Distribution on Filter Layers inside N95 Respirators by Deep Learning, *Nano Lett.*, 2021, **21**, 651–657.

5 J. Wang, L. Pan, S. Tang, J. S. Ji and X. Shi, Mask use during COVID-19: A risk adjusted strategy, *Environ. Pollut.*, 2020, **266**, 115099.

6 J. Howard, A. Huang, Z. Li, Z. Tufekci, V. Zdimal, H. M. van der Westhuizen, A. von Delft, A. Price, L. Fridman, L. H. Tang, V. Tang, G. L. Watson, C. E. Bax, R. Shaikh, F. Questier, D. Hernandez, L. F. Chu, C. M. Ramirez and A. W. Rimoin, An evidence review of face masks against COVID-19, *Proc. Natl. Acad. Sci. U. S. A.*, 2021, **118**(4), e2014564118.

7 C. M. Dugdale and R. P. Walensky, Filtration Efficiency, Effectiveness, and Availability of N95 Face Masks for COVID-19 Prevention, *JAMA Intern. Med.*, 2020, **180**(12), 1612–1613.

8 R. S. Barhate and S. Ramakrishna, Nanofibrous filtering media: Filtration problems and solutions from tiny materials, *J. Membr. Sci.*, 2007, **296**(1), 1–8.

9 F. G. Torres and G. E. De-la-Torre, Face mask waste generation and management during the COVID-19 pandemic: An overview and the Peruvian case, *Sci. Total Environ.*, 2021, **786**, 147628.

10 S. Dharmaraj, V. Ashokkumar, S. Hariharan, A. Manibharathi, P. L. Show, C. T. Chong and C. Ngamcharussrivichai, The COVID-19 pandemic face mask waste: A blooming threat to the marine environment, *Chemosphere*, 2021, **272**, 129601.

11 K. Selvaranjan, S. Navaratnam, P. Rajeev and N. Ravintherakumaran, Environmental challenges induced by extensive use of face masks during COVID-19: A review and potential solutions, *Environ. Challenges*, 2021, **3**, 100039.

12 N. U. Benson, D. E. Bassey and T. Palanisami, COVID pollution: impact of COVID-19 pandemic on global plastic waste footprint, *Heliyon*, 2021, **7**(2), e06343.

13 W. W.-F. Leung and Q. Sun, Charged PVDF multilayer nanofiber filter in filtering simulated airborne novel coronavirus (COVID-19) using ambient nano-aerosols, *Sep. Purif. Technol.*, 2020, **245**, 116887.

14 A. Palika, A. Armanious, A. Rahimi, C. Medaglia, M. Gasbarri, S. Handschin, A. Rossi, M. O. Pohl, I. Busnadiego, C. Gübeli, R. B. Anjanappa, S. Bolisetty, M. Peydayesh, S. Stertz, B. G. Hale, C. Tapparel, F. Stellacci and R. Mezzenga, An antiviral trap made of protein nanofibrils and iron oxyhydroxide nanoparticles, *Nat. Nanotechnol.*, 2021, **16**(8), 918–925.

15 S. Jeong, H. Cho, S. Han, P. Won, H. Lee, S. Hong, J. Yeo, J. Kwon and S. H. Ko, High Efficiency, Transparent, Reusable, and Active PM2.5 Filters by Hierarchical Ag Nanowire Percolation Network, *Nano Lett.*, 2017, **17**(7), 4339–4346.

16 M. Xia, Z. Yao, Z. Xiong, Y. Wu, P. Cheng, Q. Cheng, J. Xu, X. Wang, K. Liu and D. Wang, High Efficiency Antibacterial, Moisture Permeable, and Low Temperature Comfortable Janus Nanofiber Membranes for High Performance Air Filters and Respiration Monitoring Sensors, *Adv. Mater. Interfaces*, 2023, **10**(8), 2201952.

17 A. A. Jazie, A. J. Albaaji and S. A. Abed, A review on recent trends of antiviral nanoparticles and airborne filters: special insight on COVID-19 virus, *Air Qual., Atmos. Health*, 2021, **14**(11), 1811–1824.

18 B. Chen, S. Xiang and G. Qian, Metal–Organic Frameworks with Functional Pores for Recognition of Small Molecules, *Acc. Chem. Res.*, 2010, **43**(8), 1115–1124.

19 H. Xiao, Z.-X. Low, D. B. Gore, R. Kumar, M. Asadnia and Z. Zhong, Porous metal–organic framework-based filters: Synthesis methods and applications for environmental remediation, *Chem. Eng. J.*, 2022, **430**, 133160.

20 J. Lee, J. Jang, J. Kim and S.-H. Lim, A recyclable indoor air filter system based on a photocatalytic metal–organic framework for the removal of harmful volatile organic compounds, *Chem. Eng. J.*, 2022, **430**, 132891.

21 Y. Zhang, X. He, Z. Zhu, W.-N. Wang and S.-C. Chen, Simultaneous removal of VOCs and PM2.5 by metal-organic framework coated electret filter media, *J. Membr. Sci.*, 2021, **618**, 118629.

22 R. Varghese, S. Salvi, P. Sood, J. Karsiya and D. Kumar, Carbon nanotubes in COVID-19: A critical review and prospects, *Colloid Interface Sci. Commun.*, 2022, **46**, 100544.

23 S. Lee, J.-S. Nam, J. Han, Q. Zhang, E. I. Kauppinen and I. Jeon, Carbon Nanotube Mask Filters and Their Hydrophobic Barrier and Hyperthermic Antiviral Effects on SARS-CoV-2, *ACS Appl. Nano Mater.*, 2021, **4**(8), 8135–8144.

24 L. Issman, B. Graves, J. Terrones, M. Hosmillo, R. Qiao, M. Glerum, S. Yeshurun, M. Pick, I. Goodfellow, J. Elliott and A. Boies, Filtration of viral aerosols via a hybrid carbon nanotube active filter, *Carbon*, 2021, **183**, 232–242.

25 W. G. Lindsley, S. B. Martin Jr., R. E. Thewlis, K. Sarkisian, J. O. Nwoko, K. R. Mead and J. D. Noti, Effects of Ultraviolet Germicidal Irradiation (UVGI) on N95 Respirator Filtration Performance and Structural Integrity, *J. Occup. Environ. Hyg.*, 2015, **12**(8), 509–517.

26 W. Yim, D. Cheng, S. H. Patel, R. Kou, Y. S. Meng and J. V. Jokerst, KN95 and N95 Respirators Retain Filtration Efficiency despite a Loss of Dipole Charge during Decontamination, *ACS Appl. Mater. Interfaces*, 2020, **12**(49), 54473–54480.

27 S. Rengasamy, A. Miller, E. Vo and B. C. Eimer, Filter Performance Degradation of Electrostatic N95 and P100 Filtering Facepiece Respirators by Dioctyl Phthalate Aerosol Loading, *J. Eng. Fibers Fabr.*, 2013, **8**(3), 155892501300800307.

28 H. Bai, X. Qian, J. Fan, Y. Shi, Y. Duo, C. Guo and X. Wang, Theoretical Model of Single Fiber Efficiency and the Effect of Microstructure on Fibrous Filtration Performance: A Review, *Ind. Eng. Chem. Res.*, 2021, **60**(1), 3–36.

29 B. V. Ramarao, C. Tien and S. Mohan, Calculation of single fiber efficiencies for interception and impaction with superposed brownian motion, *J. Aerosol Sci.*, 1994, **25**(2), 295–313.

30 Y. Tang, K. L. Yeo, Y. Chen, L. W. Yap, W. Xiong and W. Cheng, Ultralow-density copper nanowire aerogel monoliths with tunable mechanical and electrical properties, *J. Mater. Chem. A*, 2013, **1**(23), 6723–6726.

31 D. A. Gilbert, E. C. Burks, S. V. Ushakov, P. Abellan, I. Arslan, T. E. Felter, A. Navrotsky and K. Liu, Tunable Low Density Palladium Nanowire Foams, *Chem. Mater.*, 2017, **29**(22), 9814–9818.

32 F. Qian, P. C. Lan, M. C. Freyman, W. Chen, T. Kou, T. Y. Olson, C. Zhu, M. A. Worsley, E. B. Duoss, C. M. Spadaccini, T. Baumann and T. Y.-J. Han, Ultralight Conductive Silver Nanowire Aerogels, *Nano Lett.*, 2017, **17**(12), 7171–7176.

33 F. Muench, Metal Nanotube/Nanowire-Based Unsupported Network Electrocatalysts, *Catalysts*, 2018, **8**(12), 597.

34 E. C. Burks, D. A. Gilbert, P. D. Murray, C. Flores, T. E. Felter, S. Charnvanichborikarn, S. O. Kucheyev, J. D. Colvin, G. Yin and K. Liu, 3D Nanomagnetism in Low Density Interconnected Nanowire Networks, *Nano Lett.*, 2021, **21**, 716–722.

35 D. Bhattacharya, Z. Chen, C. J. Jensen, C. Liu, E. C. Burks, D. A. Gilbert, X. Zhang, G. Yin and K. Liu, 3D Interconnected Magnetic Nanowire Networks as Potential Integrated Multistate Memristors, *Nano Lett.*, 2022, **22**(24), 10010–10017.

36 J. Malloy, A. Quintana, C. J. Jensen and K. Liu, Efficient and Robust Metallic Nanowire Foams for Deep Submicrometer Particulate Filtration, *Nano Lett.*, 2021, **21**(7), 2968–2974.

37 G. Grass, C. Rensing and M. Solioz, Metallic Copper as an Antimicrobial Surface, *Appl. Environ. Microbiol.*, 2011, **77**(5), 1541–1547.

38 T. Wang, P. Berrill, J. B. Zimmerman and E. G. Hertwich, Copper Recycling Flow Model for the United States Economy: Impact of Scrap Quality on Potential Energy Benefit, *Environ. Sci. Technol.*, 2021, **55**(8), 5485–5495.

39 K. Liu, K. Nagodawithana, P. C. Searson and C. L. Chien, Perpendicular giant magnetoresistance of multilayered Co/Cu nanowires, *Phys. Rev. B: Condens. Matter Mater. Phys.*, 1995, **51**(11), 7381.

40 J. Wong, P. Greene, R. K. Dumas and K. Liu, Probing magnetic configurations in Co/Cu multilayered nanowires, *Appl. Phys. Lett.*, 2009, **94**(3), 032504.

41 J. Malloy, K. Liu, A. Quintana and C. J. Jensen, Nanoporous Metal Foam: Efficient and Reusable Submicron Filtration Media, *Adv. Mater. Processes*, 2021, **179**(6), 28–31.

42 J.-P. Bonnet, F. Topin and L. Tadrist, Flow Laws in Metal Foams: Compressibility and Pore Size Effects, *Transp. Porous Media*, 2008, **73**(2), 233–254.

43 T. Xia, Y. Bian, L. Zhang and C. Chen, Relationship between pressure drop and face velocity for electrospun nanofiber filters, *Energy Build.*, 2018, **158**, 987–999.

44 R. Brown, in *Air Filtration: An Integrated Approach to the Theory and Applications of Fibrous Filters*, Pergamon Press, 1st edn, 1993.

45 T. Miyagi, Viscous Flow at Low Reynolds Numbers past an Infinite Row of Equal Circular Cylinders, *J. Phys. Soc. Jpn.*, 1958, **13**(5), 493–496.

46 R. M. Eninger, T. Honda, A. Adhikari, H. Heinonen-Tanski, T. Reponen and S. A. Grinshpun, Filter performance of n99

and n95 facepiece respirators against viruses and ultrafine particles, *Ann. Occup. Hyg.*, 2008, **52**(5), 385–396.

47 S. Rajupet, DLVO Interactions between Particles and Rough Surfaces: An Extended Surface Element Integration Method, *Langmuir*, 2021, **37**(45), 13208–13217.

48 C. Jin, S. D. Normani and M. B. Emelko, Surface Roughness Impacts on Granular Media Filtration at Favorable Deposition Conditions: Experiments and Modeling, *Environ. Sci. Technol.*, 2015, **49**(13), 7879–7888.

49 R. Al-Attabi, Y. Morsi, W. Kujawski, L. Kong, J. A. Schütz and L. F. Dumée, Wrinkled silica doped electrospun nano-fiber membranes with engineered roughness for advanced aerosol air filtration, *Sep. Purif. Technol.*, 2019, **215**, 500–507.

50 C. J. Drummond and D. Y. C. Chan, van der Waals Interaction, Surface Free Energies, and Contact Angles: Dispersive Polymers and Liquids, *Langmuir*, 1997, **13**(14), 3890–3895.

51 N. J. Kennedy and W. C. Hinds, Release of Simulated Anthrax Particles from Disposable Respirators, *J. Occup. Environ. Hyg.*, 2004, **1**(1), 7–10.

52 A. F. Murray, D. Bryan, D. A. Garfinkel, C. S. Jorgensen, N. Tang, W. Liyanage, E. A. Lass, Y. Yang, P. D. Rack, T. G. Denes and D. A. Gilbert, Antimicrobial properties of a multi-component alloy, *Sci. Rep.*, 2022, **12**(1), 21427.

53 H. T. Michels, Copper's Conductivity and Antimicrobial Properties Inspire Renewed Interest, *Adv. Mater. Processes*, 2020, (July/August), 1.